Geoscience Frontiers xxx (2016) 1–11

HOSTED BY

ELSEVIER

Contents lists available at ScienceDirect

China University of Geosciences (Beijing)

Geoscience Frontiers

journal homepage: www.elsevier.com/locate/gsf

Research paper

PGE mineralization and melt composition of chromitites in Proterozoic ophiolite complexes of Eastern Sayan, Southern Siberia

O. Kiseleva [a,*], S. Zhmodik [a,b]

[a] V.S. Sobolev, Institute of Geology and Mineralogy SB RAS, Novosibirsk, Russia
[b] Novosibirsk State University, Novosibirsk, Russia

ARTICLE INFO

Article history:
Received 4 December 2015
Received in revised form
26 February 2016
Accepted 14 April 2016
Available online xxx

Keywords:
Chromitites
PGE mineralization
Os-Ir-Ru and Pt-Pd patterns
Ophiolite
Eastern Sayan
Parental melt

ABSTRACT

The Ospino-Kitoi and Kharanur ultrabasic massifs represent the northern and southern ophiolite branches respectively of the Upper Onot ophiolitic nappe and they are located in the southeastern part of the Eastern Sayan (SEPES ophiolites). Podiform chromitites with PGE mineralization occur as lensoid pods within dunites and rarely in harzburgites or serpentinized peridotites. The chromitites are classified into Type I and Type II based on their $Cr^{\#}$. Type I ($Cr^{\#} = 59–85$) occurs in both northern and southern branches, whereas type II ($Cr^{\#} = 76–90$) occurs only in the northern branch. PGE contents range from $\sum$PGE 88–1189 ppb, Pt/Ir 0.04–0.42 to $\sum$PGE 250–1700 ppb, Pt/Ir 0.03–0.25 for type I chromitites of the northern and southern branches respectively. The type II chromitites of the northern branch have $\sum$PGE contents higher than that of type I (468–8617 ppb, Pt/Ir 0.1–0.33). Parental melt compositions, in equilibrium with podiform chromitites, are in the range of boninitic melts and vary in Al_2O_3, TiO_2 and FeO/MgO contents from those of type I and type II chromitites. Calculated melt compositions for type I chromitites are $(Al_2O_3)_{melt} = 10.6–13.5$ wt.%, $(TiO_2)_{melt} = 0.01–0.44$ wt.%, $(Fe/Mg)_{melt} = 0.42–1.81$; those for type II chromitites are: $(Al_2O_3)_{melt} = 7.8–10.5$ wt.%, $(TiO_2)_{melt} = 0.01–0.25$ wt.%, $(Fe/Mg)_{melt} = 0.5–2.4$. Chromitites are further divided into Os-Ir-Ru (I) and Pt-Pd (II) based on their PGE patterns. The type I chromitites show only the Os-Ir-Ru pattern whereas type II shows both Os-Ir-Ru and Pt-Pd patterns. PGE mineralization in type I chromitites is represented by the Os-Ir-Ru system, whereas in type II it is represented by the Os-Ir-Ru-Rh-Pt system. These results indicate that chromitites and PGE mineralization in the northern branch formed in a suprasubduction setting from a fluid-rich boninitic melt during active subduction. However, the chromitites and PGE mineralization of the southern branch could have formed in a spreading zone environment. Mantle peridotites have been exposed in the area with remnants of mantle-derived reduced fluids, as indicated by the occurrence of widespread highly carbonaceous graphitized ultrabasic rocks and serpentinites with up to 9.75 wt.%. Fluid inclusions in highly carbonaceous graphitized ultrabasic rocks contain CO, CO_2, CH_4, N_2 and the $\delta^{13}C$ isotopic composition (−7.4 to −14.5‰) broadly corresponds to mantle carbon.

1. Introduction

Chromitites and PGE mineralization in ophiolite complexes have been studied by many researchers worldwide (Maurel and Maurel, 1982; Dick and Bullen, 1984; Barnes et al., 1985; Nakagawa and Franco, 1997; Ballhaus, 1998; Barnes and Roeder, 2001; Kamenetsky et al., 2001; Andrews and Brenan, 2002; Ahmed and Arai, 2003; Garrutti, 2004; Rollinson, 2008; Gonzáles-Jimenéz et al., 2011; Ahmed 2013 and others). The PGE distribution and abundance, as well as chromium spinel chemistry are useful indicators of the degree of partial melting, melt-rock/melt interaction, parental melt composition and sulfur saturation of the primary melts (Dick and Bullen, 1984; Barnes et al., 1985; Rehkämper et al., 1997; Ballhaus, 1998; Barnes and Roeder, 2001; Kamenetsky et al., 2001; Naldrett, 2010; Derbyshire et al., 2013). The Ir-subgroup is more dominant in podiform chromitites (IPGE = Os, Ir, Ru) than the Pd subgroup (PPGE = Rh, Pt, Pd) (Zhou et al., 1998; Ahmed and Arai, 2003). However, chromitites with both Pt- and Pd-rich mineralization have also been reported (Prichard and Lord, 1993; Prichard et al., 1996). The paragenesis of

* Corresponding author.
E-mail addresses: Kiseleva_on@igm.nsc.ru (O. Kiseleva), Zhmodik@igm.nsc.ru (S. Zhmodik).
Peer-review under responsibility of China University of Geosciences (Beijing).

http://dx.doi.org/10.1016/j.gsf.2016.04.003

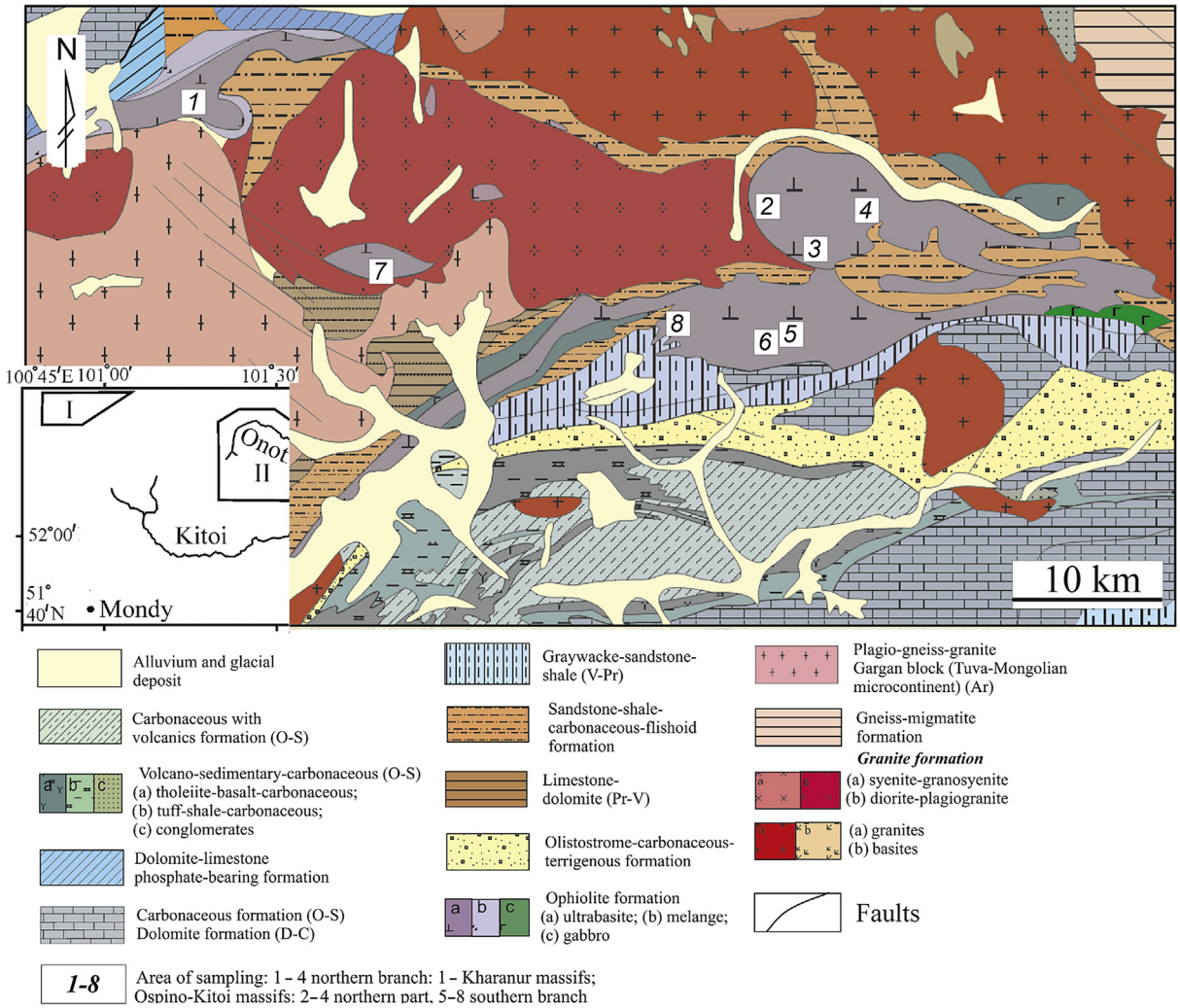

Figure 1. Geological map of part of the Eastern Sayan region (after Geology and ore-bearing zones of Eastern Sayan, 1989).

platinum group minerals (PGM) in chromitites is also useful to determine the temperature and fS_2 in magmatic systems (Barnes et al., 1985; Liipo et al., 1995; Nakagawa and Franco, 1997; Ahmed and Arai, 2002; Andrews and Brenan, 2002; Ahmed, 2007; Rollinson, 2008; Uysal et al., 2009; Grieco et al., 2012). Primary PGM changes to secondary PGM in the post-magmatic stage due to alteration at relatively low temperatures (Garuti and Zaccarini, 1997; Tsoupas and Economou-Eliopoulos, 2008; Derbyshire et al., 2013; Kiseleva et al., 2014).

The podiform chromitites and PGE mineralization of the ultrabasic massifs and ophiolite complexes within the Central Asian fold belt (Altai-Sayan region) have been investigated in some previous studies, including the ultrabasic massifs in ophiolite complexes of Tuva (Agafonov et al., 1993), the West Sayan–Kalninsky ultrabasic massif (Podlipsky et al., 2004), and the eastern Sayan–Ospino-Kitoi ultrabasic massif (Orsoev et al., 2001; Zhmodik et al., 2004, 2006; Kiseleva et al., 2014).

This study investigates the chemical features of the PGE mineralization and the parental melt compositions for chromitites of southeastern part of eastern Sayan (SEPES) ophiolites. We attempt to evaluate the physico-chemical conditions for different segments of Proterozoic oceanic lithosphere of Paleoasian Ocean, based on the chemical composition of podiform chromitites and PGM. Further, we have used published (Kiseleva et al., 2014) and new data on the chemical composition of Cr-spinel and PGM including 77 samples from Ospino-Kitoi and Kharanur ultrabasic massifs for discussion and interpretations.

2. Geological background

The eastern Sayan Mountain system is part of the Central Asian Orogenic Belt of accretion-collision origin. In the southeastern part of the eastern Sayan, Franciscan-type ophiolite complexes are common. They are characterized by spatial association of tectonic sheets, klippes and fragments of ancient oceans and marginal basins of different ages (Dilek, 2003).

The Proterozoic SEPES ophiolites are part of the Central Asian Orogenic Belt and are segments of oceanic lithosphere of the Paleoasian Ocean. The SEPES ophiolites are divided into southern and northern branches, which extend for more than 100 km. These branches form the Gargan block, which is part of the Archean Tuva-Mongolian microcontinent (Fig. 1). Ophiolite series and chemistry of rocks suggest three genetic types of different ages: (1) oceanic – Southern belt, >1200–1100 Ma; (2) island-arc – Northern or Dunzhugur belt, 1035–850 Ma; (3) back-arc – Shigna-Shishkhid belt, 850–800 Ma (Dobretsov and Ignatovich, 1989; Zhmodik et al., 2006; Kuźmichev and Larionov, 2013). The SEPES ophiolites are of two types. In type-I ophiolites, the dikes and

Please cite this article in press as: Kiseleva, O., Zhmodik, S., PGE mineralization and melt composition of chromitites in Proterozoic ophiolite complexes of Eastern Sayan, Southern Siberia, Geoscience Frontiers (2016), http://dx.doi.org/10.1016/j.gsf.2016.04.003

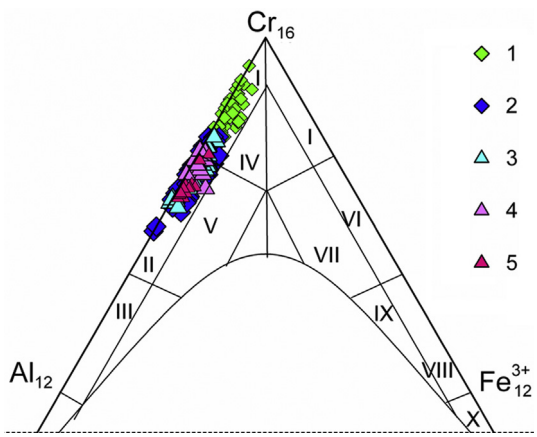

Figure 2. Classification diagram of chromium spinels from chromitites, based structural formula of spinels. Notes: composition fields: I – chromite; II – alumochromite; III – chrompicotite; IV – subferrichromite; V – subferrialumochromite; VI – ferrichromite; VII – subferrialumoferrichromite; VIII – chrome-magnetite; IX – subalumochrome-magnetite; X – magnetite (Pavlov et al., 1968). 1, 2 – chromitites from northern belt: 1 – low-Al spinels from type II chromitites, 2 – medium-Al from type I chromitites (Kiseleva et al., 2014); 3, 4, 5 – medium-Al spinels from type I chromitites from southern belt: 3 – reference for Kiseleva et al. (2014), 4 – new data, 5 – from zone of carbonized ultramafic rocks (Kiseleva et al., 2014).

volcanic rocks represent high-Ti oceanic tholeiites and MORB. Sheet-dike complex and volcanic rocks in type-II ophiolites belong to the marianite-boninite series (Dobretsov et al., 1985; Fedotova and Khain, 2002; Zhmodik et al., 2006; Kuźmichev and Larionov, 2013). The northern branch of the SEPES ophiolites consists of restitic ultrabasic massifs, lattice-banded cumulate peridotites, coarse-grained lower gabbro, medium-coarse-grained amphibole upper gabbro, sheet-dike complex, and pillow-lavas of the marianite-boninite and island-arc series. The southern branch consists of restitic ultrabasic massifs, rhythmic-banded cumulate peridotites, banded pyroxenite-anorthosite upper gabbro, small-scale upper gabbro and dikes of diabase in gabbroic and ultrabasic units. Basalts of oceanic type are found in olistoliths (Dobretsov et al., 1985).

The Ospino-Kitoi and Kharanur restitic ultrabasic massifs are part of the Upper Onot ophiolitic nappe located in southeastern part of Eastern Sayan (SEPES ophiolites). They are the largest ultramafic restite massifs in Eastern Sayan. They comprise dominantly of dunites together with harzburgites, which are often serpentinized and carbonated. Metasomatic replacements are common and rocks like listwänites and rodingites are widespread with zones of talc-carbonate and altered dunites. The Ospino-Kitoi and Kharanur ultrabasic massifs contain podiform chromitites hosted mainly by tectonically deformed dunites, rarely harzburgites. Podiform chromitites form lensoidal pods concordant with the host ultramafic rocks and occur within ore zones of 0.1–0.5 m thick and 400 m long.

3. Sample description

Seventy seven samples (weighing from 1 to 8 kg) were collected from different chromite bodies in the SEPES ophiolites (northern and southern branches). The chromite pods show both

Table 1
Representative selective scanning electron microscope analyses of Cr-spinels (wt.%) from massive chromitites (from 44 analyses).

	BC65 2-6	BC67 5-6	BC67 5-5	BC67 5-8	BC67 2-9	BC67 5-4	BC18 1-3	BC18 1-6	BC18 3-8	BC18 6-1	OK10sh 1-4
Al_2O_3	13.93	14.91	15.51	12.58	14.47	14.17	13.87	14.83	14.38	14.40	13.70
Cr_2O_3	56.59	57.88	56.45	58.95	57.92	57.26	56.74	56.31	54.52	56.80	58.36
FeO	13.00	13.60	12.96	13.57	13.30	12.70	13.57	15.09	11.79	14.06	13.59
Fe_2O_3	1.70	0.68	1.56	1.36	1.22	2.15	1.66	1.07	3.98	1.38	1.11
MnO	n.d	n.d	n.d	n.d	n.d	n.d	n.d	n.d	1.76	n.d	n.d
MgO	13.65	13.78	14.01	13.07	13.93	13.93	13.33	12.60	13.53	13.22	13.55
NiO	n.d	n.d	0.39	0.50	n.d	0.51	n.d	n.d	n.d	n.d	n.d
Total	98.86	100.85	100.88	100.02	100.84	100.73	99.17	99.91	99.96	99.85	100.31
Atomic concentration on the basis of four oxygens											
Al	0.53	0.55	0.57	0.48	0.54	0.53	0.52	0.56	0.54	0.54	0.51
Cr	1.43	1.43	1.39	1.49	1.44	1.42	1.44	1.42	1.37	1.43	1.46
Fe^{2+}	0.35	0.36	0.34	0.36	0.35	0.33	0.36	0.40	0.31	0.37	0.36
Fe^{3+}	0.04	0.02	0.04	0.03	0.03	0.05	0.04	0.03	0.10	0.03	0.03
Mn	0.00	0.00	0.00	0.00	0.00	0.00	0.00	0.00	0.05	0.00	0.00
Mg	0.65	0.64	0.65	0.62	0.65	0.65	0.64	0.60	0.64	0.63	0.64
Ni	0.00	0.00	0.01	0.01	0.00	0.01	0.00	0.00	0.00	0.00	0.00

	OK10sh 11-2	OK10sh 3-4	OK10sh 16-5	OK10an 1-1	OK10an 1-4	OK10an 6-3	OK10an 7-5	OK10an 2-5	OK10sh 1-5	OK10sh 3-3
Al_2O_3	13.13	13.91	13.00	14.30	13.81	16.12	13.98	12.55	12.68	12.41
Cr_2O_3	59.55	59.37	56.99	58.57	59.28	58.17	59.24	60.17	59.52	59.68
FeO	13.53	12.17	20.61	11.57	12.38	14.57	13.39	12.79	14.04	14.44
Fe_2O_3	0.29	0.91	0.54	1.37	0.71	0.23	0.81	1.15	0.00	0.74
MnO	n.d	n.d	n.d	n.d	n.d	n.d	n.d	n.d	n.d	n.d
MgO	13.47	14.64	8.82	15.04	14.41	13.66	13.93	14.05	12.85	12.82
NiO	n.d	n.d	n.d	n.d	n.d	n.d	n.d	n.d	n.d	n.d
Total	99.96	101.00	99.96	100.85	100.59	102.76	101.34	100.71	99.08	100.09
Atomic concentration on the basis of four oxygens										
Al	0.49	0.51	0.50	0.53	0.51	0.58	0.52	0.47	0.48	0.47
Cr	1.50	1.47	1.48	1.44	1.47	1.41	1.47	1.51	1.52	1.51
Fe^{2+}	0.36	0.32	0.57	0.30	0.33	0.37	0.35	0.34	0.38	0.39
Fe^{3+}	0.01	0.02	0.01	0.03	0.02	0.01	0.02	0.03	0.00	0.02
Mn	0.00	0.00	0.00	0.00	0.00	0.00	0.00	0.00	0.00	0.00
Mg	0.64	0.68	0.43	0.70	0.68	0.63	0.65	0.66	0.62	0.61
Ni	0.00	0.00	0.00	0.00	0.00	0.00	0.00	0.00	0.00	0.00

Notes: Cr-spinels from chromitites of new district (previously not examined) unpublished data. Analyses: BC18_3-8, OK10sh_11-2, OK10an_7-5, OK10an_2-5 – Cr-spinels contain inclusion of PGM.

Please cite this article in press as: Kiseleva, O., Zhmodik, S., PGE mineralization and melt composition of chromitites in Proterozoic ophiolite complexes of Eastern Sayan, Southern Siberia, Geoscience Frontiers (2016), http://dx.doi.org/10.1016/j.gsf.2016.04.003

disseminated and massive structures. There are veins of massive chromitites, 0.01–0.5 m thick, and 1–10 m long, which are discordant to the host ultramafic rocks. The chromitites are of massive type (>80% modal chromite). They are composed of subhedral to anhedral chromite grains up to 1–5 mm in size, mostly relatively fresh, although altered sieve-textured rims and fractures in grains are common. In the intensely brecciated chromian spinels, the grains became very fine grained and with the fractures filled with chlorite and serpentine. Fifteen grains of PGM were separated from the four samples of chromitites. Three polished grain mounts were prepared and microscopic study reveals that PGM occur as single or composite inclusions in chromite.

4. Analytical techniques

The method of determination of PGE concentration is based on pre-concentration of the platinum metals in the collector-nickel matte, selective dissolution of the sulfides in hydrochloric acid, co-precipitation of platinum metals on tellurium and transfer of noble metals to solution with a mixture of hydrochloric and nitric

Table 2
Electron microprobe analyses of platinum group minerals from new investigated massive chromite bodies of southern branch (wt.%).

		Os	Ir	Ru	Rh	Pt	Fe	Ni	Cu	As	S	Total	Crystal-chemical formula	Form of occurrence
1	BC-65_1-7	4.7	1.9	52.7	0	2.3	0.3	0.3		3.4	36.1	100.7	$Ru_{0.52}Os_{0.02}Ir_{0.01}Pt_{0.01}Ni_{0.01}S_{1.95}As_{0.05}$	Polyphase aggregate
2	BC-65_1-9	14.2	3.1	42.7	0	2.4				2.3	32.9	97.6	$Ru_{0.5}Os_{0.09}Ir_{0.02}Pt_{0.01}S_{1.96}As_{0.04}$	Polyphase aggregate
3	350_4_8-4	2.7	3.3	53.3				0.9		0.7	36.5	97.4	$Ru_{0.52}Ir_{0.02}Ni_{0.01}S_{1.99}As_{0.01}$	Polyphase aggregate
4	334_4_1-4			59.1					0.7	1.5	37.7	99	$Ru_{0.98}Cu_{0.02}S_{1.97}As_{0.03}$	Polyphase aggregate
5	OK10sh_13	66.2	31.4	2.3	–	–	0.3	–	–	0.3	–	100.5	$Os_{0.65}Ir_{0.3}Ru_{0.04}Fe_{0.01}$	Individual grain l
6	BC18_3-4_1	44.3	17.3	31.6	–	–		–	–	–	–	93.2	$Os_{0.37}Ru_{0.49}Ir_{0.14}$	Individual grain
7	BC18_3-3_1	47.9	35.4	10.7	0.9	–		–	–	–	–	94.9	$Os_{0.46}Ir_{0.33}Ru_{0.19}Rh_{0.01}$	Individual grain
8	BC67_2-3_1	53.9	35.2	5.1	–	–	0.2	–	–	–	–	94.4	$Os_{0.54}Ir_{0.35}Ru_{0.1}Fe_{0.01}$	Individual grain
9	BC18_3-4_7	62.5	6.5	15.6	–	–		0.7	–	2.2	5.8	93.3	$Os_{0.62}Ru_{0.29}Ir_{0.06}Ni_{0.02}$	Rim of grain (an.No 6)
10	OK10sh-2	47.2	39.9	10.6	0.6	–	0.5	0.2	–	–	–	99	$Os_{0.43}Ir_{0.36}Ru_{0.18}Rh_{0.01}Fe_{0.01}Ni_{0.01}$	Individual grain
11	OK10an2-1	50.9	42.4	6.5	–	–	0.8	–	–	–	–	100.6	$Os_{0.47}Ir_{0.38}Ru_{0.11}Fe_{0.02}$	Inclusion in Cr-spinel
12	OK10an2-3	43.1	36.9	1.9	–	–	0.6	0.7	–	12.3	5.2	100.7	$Os_{0.49}Ir_{0.41}Ru_{0.04}Fe_{0.02}Ni_{0.03}$	Emulsive nanoparticles in Irs
13	OK10an7-1	27.8	48.6	18.6	–	–	0.6	–	–	–	–	95.6	$Ir_{0.51}Os_{0.29}Ru_{0.19}Fe_{0.01}$	Individual grain
14	OK10sh11-1	31.9	53.9	7.9	–	–	0.9	–	–	–	–	94.6	$Ir_{0.57}Os_{0.34}Ru_{0.08}Fe_{0.01}$	inclusion in Cr-spinel
15	OK10sh17	29.4	62.2	4.6	–	–	0.6	–	–	0	0.0	96.8	$Ir_{0.64}Os_{0.31}Ru_{0.05}$	Individual grain
16	BC18_3-2_7	35.5	45.8	12.2	1.1	–	0.6	–	–	2.7	1.1	99	$Ir_{0.48}Os_{0.37}Ru_{0.13}Rh_{0.01}Fe_{0.01}$	Rim of grain (an.No 17)
17	BC18_3-2_2	23.9	55.7	13.3	–	–	4.2	–	–	0.9	0.4	98.4	$Ir_{0.57}Os_{0.25}Ru_{0.14}Fe_{0.04}$	Individual grain
18	BC18_3-2_5	26.7	48.5	5.7	–	–	1.5	0.9	–	7.9	4.1	95.3	$Ir_{0.58}Os_{0.32}Ru_{0.07}Fe_{0.02}Ni_{0.01}$	Rim of grain (an.No 17)
19	BC18_3-2	74.7	6.1	8.6	–	–		2.5	0.8	1.7	–	94.44	$Os_{0.81}Ru_{0.09}Ir_{0.07}Ni_{0.02}Cu_{0.01}$	Rim of grain (an.No 7)
20	BC18_3-3_3	70.1	9.5	7.7	–	–		–	–	3.7	1.7	92.7	$Os_{0.8}Ir_{0.1}Ru_{0.1}$	Rim of grain (an.No 7)
21	OK10an_3-4	81.5	4.8	8.3	–	–	0.7	–	–	2.4	4.5	102.2		Emulsive nanoparticles in Lr. Irs
22	OK10an7-6	100.6	3.5	2.1	–	–	0.4	–	–	2.1	0.7	109.4		Emulsive nanoparticles in Lr. Irs
23	OK10sh9-9	93.1	–	–	–	–		3.9	–	3.1	1.8	101.9	$Os_{0.96}Ni_{0.04}$	Polyphase intergrowth
24	OK10sh9-10	98.7	–	–	–	–	0.6	–	–	0.6	–	99.9	$Os_{0.94}Ni_{0.05}Fe_{0.01}$	Polyphase intergrowth
25	OK10sh9-1	99.2	–	–	–	–		2.4	–	0.2	–	101.8	$Os_{0.98}Ni_{0.02}$	Polyphase intergrowth
26	BC9_1-1_5	93.4	3.9	3.8	–	–		0.9	–	0.5	–	102.5		Emulsive nanoparticles in Irs
27	OK10an3-1	–	1.8	59.7	–	–		–	–	–	37.3	98.8	$Ru_{1.01}Ir_{0.02}S_2$	Polyphase intergrowth
28	BC18-3_3-6	9.4	11.0	43.8	–	–		–	–	5.7	27.6	97.5	$Ru_{0.92}Ir_{0.12}Os_{0.1}S_2$	Relicts in Irs
29	BC18-3_4-8	–	3.0	59.9	–	–		–	–	1.7	37.2	101.8	$Ru_1Ir_{0.02}S_2$	Rim of grain (an.No 6)
30	BC18-3_4-6	8.6	12.1	40.3	–	–		–	–	6.0	26.5	93.5	$Ru_{0.88}Ir_{0.13}Os_{0.09}S_2$	Rim of grain (an.No 6)
31	BC18-3_4-9	–	13.7	48.9	–	–		–	–	5.2	32.8	100.6	$Ru_{0.88}Ir_{0.13}S_2$	Rim of grain (an.No 6)
32	OK10an2_7-4	14.8		49.3	0	–	–	–	–	5.5	32.2	101.8	$Ru_{0.9}Os_{0.14}S_2$	Rim of grain (an.No 13)
33	349-97_3-2		6.2	47.9				1.4		1.8	31.2	88.5	$Ru_{0.56}Ir_{0.04}Ni_{0.01}S_{1.97}As_{0.03}$	Individual
34	K-37_7-1		1.6	60.7						1.0	35.6	98.9	$Ru_{0.8}Ir_{0.03}Os_{0.03}S_2$	Polyphase aggregate
35	BC-17_7	4.2	4.1	59.8	0.4						29.5	98	$Ru_{0.56}Ir_{0.04}Ni_{0.01}S_{1.97}As_{0.03}$	Individual
36	OK-162_12-1	6.3	3.8	52.2					0.8	0.9	30.3	94.3	$Ru_{0.66}Ir_{0.03}Os_{0.04}S_{1.98}As_{0.02}$	Individual
37	OK-162a_1-1	6.9	1.7	55.1			0.2	0.7		1.1	33.6	99.3	$Ru_{0.61}Os_{0.04}Ir_{0.01}S_{1.99}As_{0.01}$	Individual
38	OK-162a_5-2	2.2	2.8	50.3			0.3	1.6		5.8	35.2	98.2	$Ru_{0.49}Os_{0.01}Ir_{0.01}S_{1.92}As_{0.08}$	Polyphase aggregate
39	OK10an2_7-2	40.3	34.9	3.6	0	–	–	–	–	12.2	5.8	96.8	$Os_{0.62}Ir_{0.53}Ru_{0.1}S_{0.53}As_{0.47}$	Rim of grain (an.No 13)
40	BC18-3_4-3	11.8	41.2	6.8	0.9	3.3	–	–	–	20.3	10.9	95.2	$Ir_{0.35}Os_{0.1}Ru_{0.11}Pt_{0.03}Rh_{0.01}S_{0.56}As_{0.44}$	Rim of grain (an.No 6)
41	BC18-3_4-5	–	48.7	3.3	–	6.2	–	–	–	25.7	11.2	95.1	$Ir_{0.36}Ru_{0.05}Pt_{0.05}S_{0.5}As_{0.5}$	Rim of grain (an.No 6)
42	OK10an2_2-2	–	51.4	8.9	–	–	–	–	–	23.3	14.7	98.3	$Ir_{0.35}Ru_{0.11}S_{0.6}As_{0.4}$	Rim of grain (an.No 11)
43	OK10an2_3-2	–	56.2	3.1	–	–	0.6	–	–	24.9	12.1	96.9	$Ir_{0.41}Ru_{0.04}Fe_{0.01}S_{0.53}As_{0.47}$	Intergrowth with Lr
44	OK10an2_7-3	–	54.4	3.6	0.8	–	–	–	–	24.9	11.7	95.4	$Ir_{0.41}Ru_{0.05}Rh_{0.01}S_{0.52}As_{0.48}$	Rim of grain (an.No 13)
45	OK10sh9-2	–	58.4	2.4	0.9	–	–	2.8	–	23.2	11.5	99.2	$Ir_{0.45}Ru_{0.04}Rh_{0.01}Ni_{0.07}S_{0.54}As_{0.46}$	Polyphase intergrowth
46	OK10sh9-4	–	58.8	1.7	2.5	–	–	1.3	–	23.9	11.4	99.6	$Ir_{0.45}Ru_{0.02}Rh_{0.04}Ni_{0.03}S_{0.53}As_{0.47}$	Polyphase intergrowth
47	OK10sh9-6	–	59.1	1.8	1.3	–	–	1.6	–	24.8	11.7	100.3	$Ir_{0.44}Ru_{0.03}Rh_{0.02}Ni_{0.04}S_{0.52}As_{0.48}$	Polyphase intergrowth
48	BC9_1_1-1	–	52.8	3.5	–	5.7	–	–	–	25.2	11.7	98.9	$Ir_{0.39}Ru_{0.05}Pt_{0.04}S_{0.52}As_{0.48}$	Individual
49	BC9_1_1-2	–	59.2	0.9	1.2	0	–	0.7	–	21.8	11.3	95.1	$Ir_{0.48}Ru_{0.01}Rh_{0.02}Ni_{0.02}S_{0.55}As_{0.45}$	Individual
50	BC9_1_1-3	–	55.6	2.5	0.5	1.9	–	0.6	–	22.0	11.3	94.4	$Ir_{0.45}Ru_{0.04}Rh_{0.01}Pt_{0.02}Ni_{0.02}S_{0.55}As_{0.45}$	Individual
51	BC18-3_2-3	–	41.4	3.0	14.3	2.5	0.3	–	–	27.9	13.4	102.8	$Ir_{0.27}Rh_{0.18}Ru_{0.04}Pt_{0.02}Fe_{0.01}S_{0.53}As_{0.47}$	Rim of grain (an.No 17)
52	BC18-3_3-4	7.7	35.8	8.9	0.9	8.7	–	–	–	21.6	11.7	95.3	$Ir_{0.29}Ru_{0.14}Pt_{0.07}Rh_{0.01}S_{0.56}As_{0.44}$	Rim of grain (an.No 7)
53	BC18-3_3-5	–	50.2	4.2	1.9	–	–	1.4	–	25.0	11.1	93.8	$Ir_{0.38}Ru_{0.06}Rh_{0.03}Ni_{0.04}S_{0.51}As_{0.49}$	Rim of grain (an.No 7)
54	BC18-3_3-7	–	55.5	3.3	0.9	–	0.5	–	–	26.1	11.1	97.4	$Ir_{0.41}Ru_{0.05}Rh_{0.01}Fe_{0.01}S_{0.5}As_{0.5}$	Rim of grain (an.No 7)
55	BC18-3_2-6	–	39.0	10.3	5.6	4.7	0.8	–	–	20.7	14.5	95.6	$Ir_{0.28}Ru_{0.14}Rh_{0.07}Pt_{0.03}Fe_{0.02}S_{0.62}As_{0.38}$	Rim of grain (an.No 17)
56	BC18-3_2-4	23.5	52.8	7.2	–	–	1.6	0.7	–	5.6	2.9	94.3	$Ir_{1.65}Os_{0.74}Ru_{0.42}Fe_{0.17}Ni_{0.07}S_{0.55}As_{0.45}$	Rim of grain (an.No 17)

Notes: – not detected; *northern branch*: 1–4 laurites; *southern branch (new data)*: 5–18 solid-solution (Os-Ir-Ru); 19–26 native osmium; 27–38 laurite(RuS_2); 39–56 solid-solution irarsite-osarsite-ruarsite (IrAsS-RuAsS-OsAsS); Lr – laurite, Irs – irarsite.

Please cite this article in press as: Kiseleva, O., Zhmodik, S., PGE mineralization and melt composition of chromitites in Proterozoic ophiolite complexes of Eastern Sayan, Southern Siberia, Geoscience Frontiers (2016), http://dx.doi.org/10.1016/j.gsf.2016.04.003

acids. Determination of elemental concentrations in the resulting solution is carried out by ICP-MS (STE 35-12-241-2001) in the Department of Analytical Researches, Federal State Unitary Enterprise "Central Research Institute of Geological Prospecting for Base and Precious Metals", Moscow. The concentration of PGE in chromitites was determined by assay-mass spectrometry with inductively coupled plasma and preliminary assay using a Ni matte as a collector. The chemical composition of the chromite and PGE minerals (polished chromite sections, polished blocks, and epoxy mounts of the heavy mineral separates) were analyzed by quantitative X-ray microanalysis using a Camebax-Micro microprobe. The analytical conditions for Camebax-Micro microprobe were as follows: 20 kV accelerating voltage, beam current 100 nA and 10 s counting time. Detection limits were generally about 0.03–0.01 wt.%. In addition fine grains of PGE minerals were analyzed by Tescan-MIRA 3 LMU scanning electron microscope with an INCA Energy 450+ micro-analyzer based on the Oxford Instruments NanoAnalysis X-MAX 80 system (UK) (Cr-spinel and platinum group minerals) with the following conditions: 20 kV accelerating voltage, 1600 pA beam current, 20 s counting time. Native minerals, synthetic crystalline phases, metals and metal alloys were used as standards, with the maximum relative errors for PGM: 0.48 wt.% for Ru, 0.36 wt.% for Os, 0.38 wt.% for Ir and Rh, 0.13 wt.% for Pt, 0.17 wt.% for Pd.

5. Results

5.1. Composition of chrome-spinel

Cr-spinel in the chromitites from the northern branch has compositions ranging from alumochromite to chromite (Fig. 2). Chromitites from the southern branch contain only alumochromite (Table 1, Kiseleva et al., 2014). The chromitites with alumochromite ($Al/(Al + Cr + Fe^{3+}) = 20–40$, $Cr^{\#} = 59–85$) are called *type I chromitites* and are found in both northern and southern branches, whereas those with ($Al/(Al + Cr + Fe^{3+}) = 9–21$, $Cr^{\#} = 76–90$) are called *type II chromitites* (Kiseleva et al., 2014, new original data). Cr-spinels from chromitites in the southern branch have more homogeneous compositions (Tables 1 and 2).

5.2. Distribution of PGE in chromite bodies

The common PGE patterns (Fig. 3A, B) are Os-Ir-Ru (Type I) and Pt-Pd (Type II). *Type I chromitites* (mid-Al Cr-spinels) show uniform chondrite-normalized PGE patterns with a negative slope from Ru to Pt (similar to the worldwide ophiolitic chromitite). The PGE patterns in *type II chromitites* show a gentle negative slope, being enriched in both IPGE (Os, Ir, Ru) and PPGE (Rh, Pt, Pd) (Kiseleva et al., 2014). The patterns of PGE for type I chromitites are similar to those from the IPGE in podiform chromitites found in ophiolites of Wadi Al Hwanet (northwestern Saudi Arabia), Oman, Veria (northern Greece), and Shetland. The PGE patterns in type II chromitites from the northern branch are similar to those in high IPGE and PPGE podiform chromitites from the same ophiolite complexes (Prichard et al., 1996; Ahmed et al., 2012; O'Driscoll et al., 2012) (Fig. 3C).

5.3. Morphology and mineral paragenesis of platinum group minerals (PGM)

For the *type I chromitites* the PGM are represented by the *Os-Ir-Ru* system. In *type II chromitites* PGM are represented by *Os-Ir-Ru-Rh-Pt* system (Fig. 4A, B). PGE mineralization is well documented and described by Kiseleva et al. (2014). Here we present new data on PGM. Chemical compositions and crystallochemical formulas of PGM are listed in Table 2 and Fig. 5A, B. The chromitites are dominated by Os-Ir-Ru minerals.

The *solid-solutions (Os-Ir-Ru)* (Fig. 5A) correspond to osmium, iridium and ruthenium alloys or inter-metallides (Harris and Cabri, 1991). They occur as inclusions (from 5 to 80 μm) in Cr-spinels (Fig. 6A, B, E, G), and as individual grains (from 10 to 65 μm) in heavy mineral fraction which are rounded, irregular or cubic crystals. Impurities in Os-Ir-Ru solid solutions are Rh, Fe, and Ni. The solid solutions of Os-Ir-Ru are often replaced by irarsite-osarsite-ruarsite and irarsite-hollingworthite. In one grain, native osmium (Fig. 6D) is overgrown by awaruite (Ni_3Fe). Zonal substitutions are noticed in two grains, where iridium with high Ru content (18 wt.%) is replaced by laurite in the rim, whereas near the center it is substituted by irarsite (Fig. 6B).

Native osmium (Os > 70 wt.%) occurs as dispersed nanoparticles in irarsite, laurite and as intergrowths (from 5 to 15 μm) and nanoparticles in polyphase aggregates (Fig. 6) with irarsite, heazlewoodite (Ni_3S_2), horomanite ($Fe_6Ni_3S_8$) and orselite ($Ni_{5-x}As_2$).

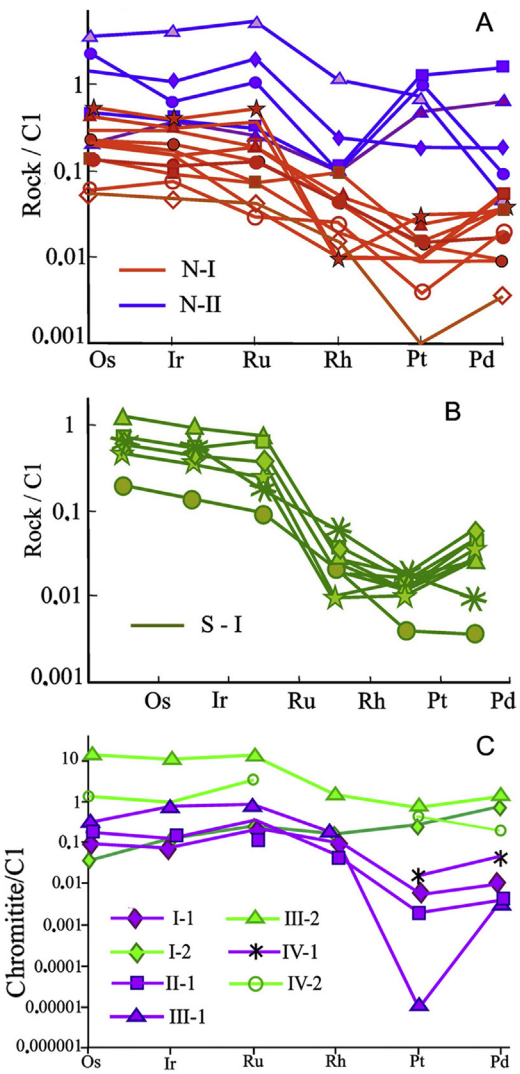

Figure 3. Chondrite-normalized PGE patterns for the massive chromite bodies (Kiseleva et al., 2014; Zhmodik et al., 2014). (A) Northern branch, N-I – (Os-Ir-Ru) fractionation type, N-II – (Pt-Pd) type; (B) southern branch, S-I – (Os-Ir-Ru) fractionation type; (C) from world-wide ophiolites complexes 1 – high IPGE, 2 – high IPGE and PPGE: I – Wadi Al Hwanet, northwestern Saudi Arabia (Ahmed et al., 2012); II – Oman (Prichard et al., 1996); III – Veria, Greece (Tsoupas and Economou-Eliopoulos, 2008); IV – Shetland ophiolite complexe, Scotland (O'Driscoll et al., 2012).

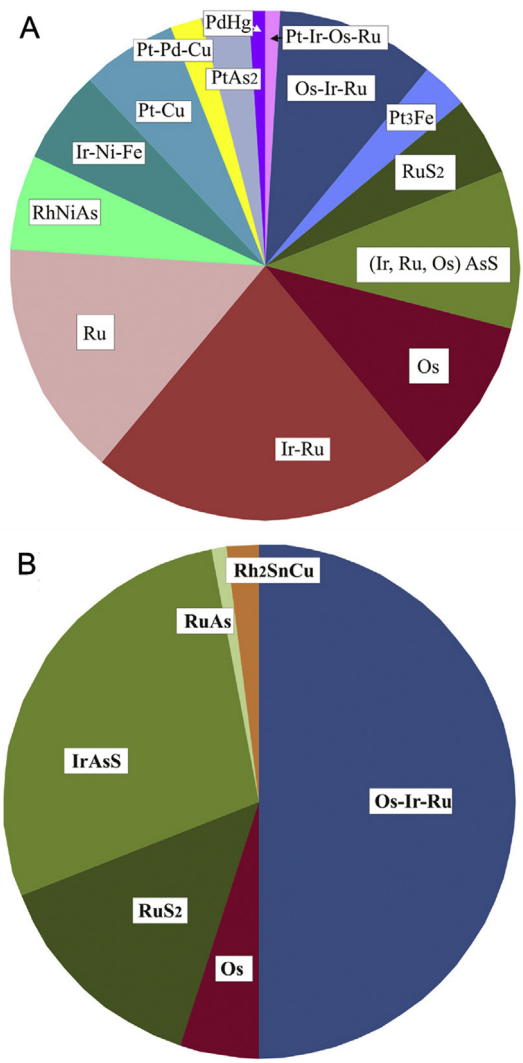

Figure 4. PGM association in chromite bodies (Kiseleva et al., 2014; Zhmodik et al., 2014): (A) northern branch; (B) southern branch.

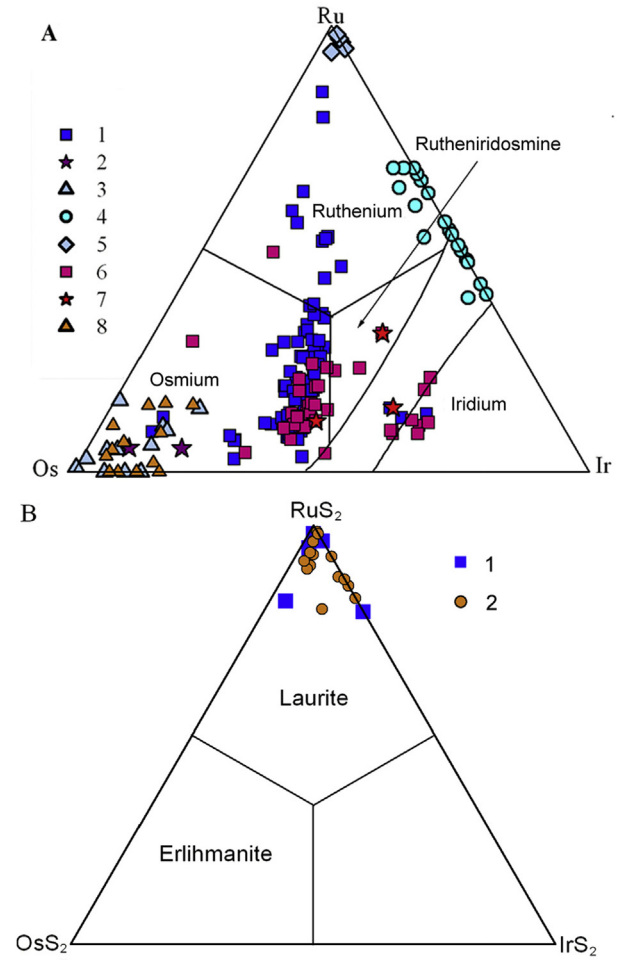

Figure 5. Diagram for compositions of PGE minerals (A) in the Os-Ir-Ru system – *northern branch*: (1) high-temperature (Os-Ir-Ru) solid solution, (2) lamellae (Os-Ir-Ru) in Pt_3Fe, (3) native osmium in (Os-Ir-Ru) zoned phases (Kiseleva et al., 2014), in (Os-Ir-Ru) sulfides, sulfoarsenides, polyphase aggregates, (4) (Ir-Ru) inclusions in RhNiAs, polyphase aggregates, (5) native ruthenium in (Os-Ir-Ru) zoned phases (Kiseleva et al., 2014), polyphase aggregates; *southern branch*: (6) high-temperature (Os-Ir-Ru) solid solution, (7) inclusion in Cr-spinels, (8) native osmium in (Os-Ir-Ru) sulfides, sulfoarsenides, polyphase aggregates; (B) laurite-erlihmanite: (1) northern branches, (2) southern branch (Kiseleva et al., 2014; new data).

Laurite (RuS_2) occurs in the serpentinized matrix in intergranular space of Cr-spinel forming particulates of irregular shape (5 μm × 12 μm). Composition of the laurite is shown in Table 2, Fig. 5B. Laurite is replaced by irarsite (Fig. 6G, H). Similar to irarsite, laurite contains dispersed particulates of native osmium.

Sulfoarsenides of Ir, Ru, Ru, Rh form phases of variable composition with irarsite as the dominant phase (Table 2). In addition, solid solutions such as irarsite-hollingworthite IrAsS-RhAsS and irarsite-osarsite-ruarsite IrAsS-OsAsS-RuAsS also occur. In the sulfoarsenides impurities of Pt, Rh, Ni, and Sb were detected. Sulfoarsenides occur as individual irregular shaped grains up to 50 μm (Fig. 6). They also form replacement rims ~20 μm in width on Os-Ir-Ru solid solution grains (Fig. 6). Sulfoarsenides form polyphase aggregates with native osmium, heazlewoodite (Ni_3S_2), orselite ($Ni_{5-x}As_2$) and horomonite ($Fe_6Ni_3S_8$) (Fig. 6A–L).

6. Discussion

6.1. Parental melt of chromitites

The compositions of chromium spinels from podiform chromitites and their FeO, MgO, Al_2O_3, TiO_2 contents, are considered as the function of the parental melt composition. Chemical features allow characterization of spinels, which form from magmas of different composition (Maurel and Maurel, 1982; Dick and Bullen, 1984; Melcher et al., 1997; Zhou et al., 1998; Kamenetsky et al., 2001; Rollinson, 2008; González-Jiménez et al., 2011 and others). The chromitites of this study show chemical characteristics typical of podiform chromite deposits (Kiseleva et al., 2014).

Cr-spinels from the chromitite bodies of the northern and southern branches have discrete bimodal chemical compositions. Two Cr-spinels groups are recognized (Kiseleva et al., 2014 and new data). Cr-spinels from type I chromitites have similar chemical characteristic to Cr-spinels from ophiolitic complexes worldwide (Fig. 7). Chemical composition of high-Cr chromium spinels (type II chromitites) and the Al_2O_3 content of their parental melts are similar to those of Cr-spinels from Wadi Al Hwanet ophiolites (Saudi Arabia) (Ahmed et al., 2012). According to their $Cr^{\#}$–$Mg^{\#}$ ratios, the majority of Cr-spinels fall within the boninitic field (Fig. 7A). The $Mg^{\#}$ values show dispersion and some Cr-spinels correspond to the Alaskan-type of intrusions. On the Al_2O_3–Fe^{2+}/Fe^{3+} discrimination diagram, the Cr-spinels from type I chromitites of the northern and southern branches partly fall within the MORB peridotites field, whereas the

Please cite this article in press as: Kiseleva, O., Zhmodik, S., PGE mineralization and melt composition of chromitites in Proterozoic ophiolite complexes of Eastern Sayan, Southern Siberia, Geoscience Frontiers (2016), http://dx.doi.org/10.1016/j.gsf.2016.04.003

type II chromitites, plot within the SSZ peridotites field (Fig. 7B). Cr-spinels in chromitites from the northern branch show wide variations in TiO_2 values that could be the result of interaction with Ti-rich melts. The bimodal geochemical characteristics of chromitites in terms of their $Cr^{\#}$, and variation of composition TiO_2 and FeO, of Cr-spinels may be attributed to different degrees of partial melting, variations of magma composition, and secondary stages of melting. We estimated the Al_2O_3, TiO_2 contents and FeO/MgO of the parental melt composition in equilibrium with the podiform chromitites (Table 3, Fig. 7C). The contents of Al_2O_3, TiO_2, FeO, and MgO in

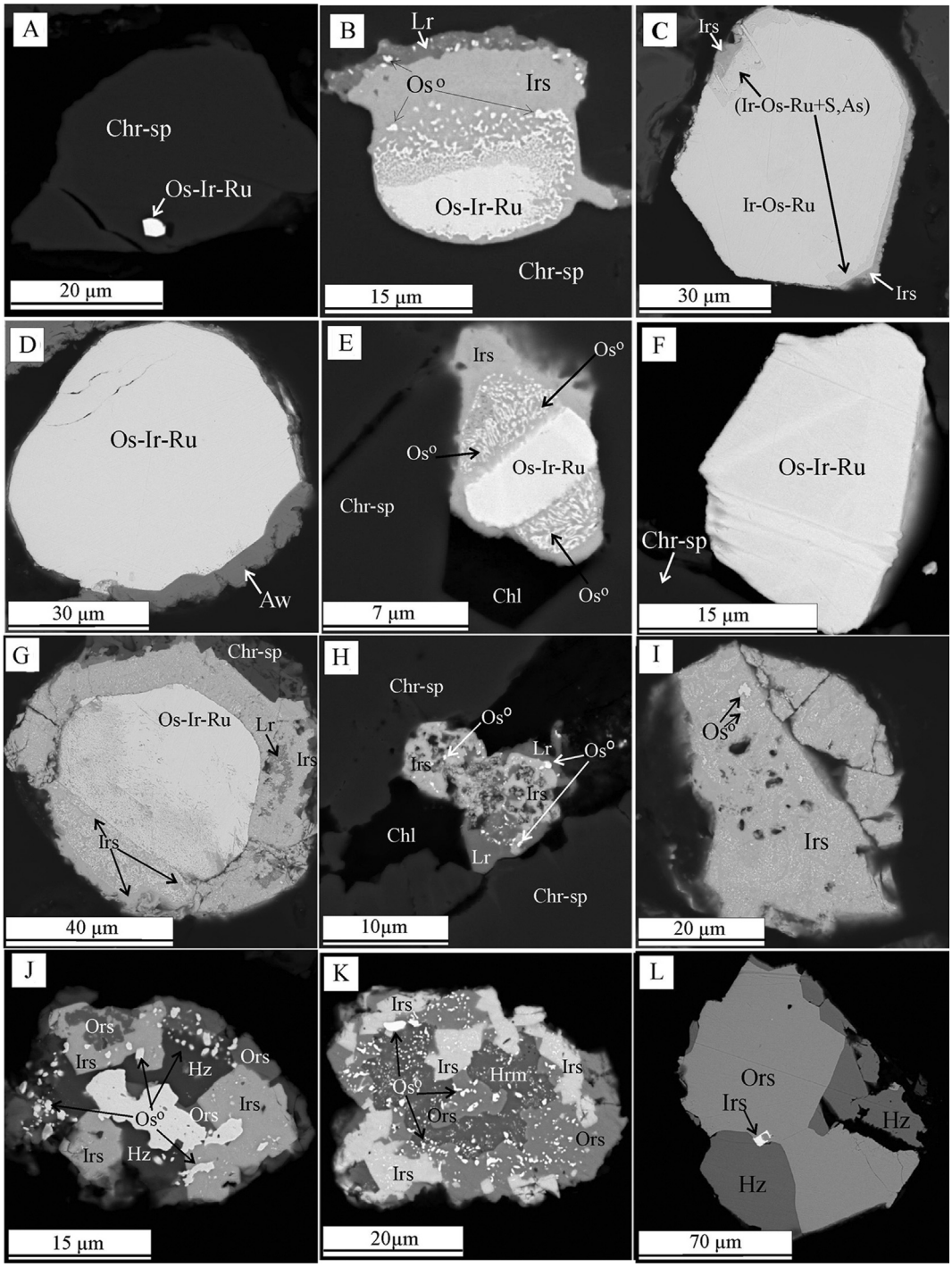

Figure 6. Photomicrographs of platinum group minerals from chromitites in BSE (new studied chromite bodies from southern branch) (A) inclusion solid solution (Os-Ir-Ru) in Cr-spinels (an.No. 14); (B) inclusion solid solution (Os-Ir-Ru) in Cr-spinels with zonal replacement by irarsite and laurite and emulsive nanoparticles of native osmium in irarsite and laurite (an.Nos. 13, 22, 32, 39, 44); (C) euhedral grain solid solution (Os-Ir-Ru) with rim of irarsite (an.Nos. 16, 17, 18, 51, 56); (D) rounded grain solid solution (Os-Ir-Ru) with awaruite owergrowth (an.No. 8); (E) inclusion Os-Ir-Ru in Cr-spinels surrounded by irarsite with nanoparticles of native osmium (an.Nos. 11, 12, 42); (F) individual grain (Os-Ir-Ru) (an.No. 15); (G) individual grain (Os-Ir-Ru) surrounded by irarsite (an.Nos. 7, 19, 20, 28, 52); (H) intergrowth porous grains of laurite and irarsite in crack with chlorite matrix (an.Nos. 21, 27, 43); (I) irregular grain of irarsite with emulsive nanoparticles of native osmium (an.Nos. 22, 38, 39, 40); (J) polyphase aggregate (an.Nos. 24, 25, 45, 46, 47); (K) polyphase aggregate; (L) intergrowth irarsite, orselite, heazlewoodite. Notes: Chr-sp – chromium spinel, Os^{o} – native osmium, Lr – laurite, Irs – irarsite, Hz – heazlewoodite (Ni_3S_2), Hrm – horomanite ($Fe_6Ni_3S_8$), Ors – orselite ($Ni_{5-x}As_2$). Comments: 'an.No.' means number of analysis in Table 2.

Please cite this article in press as: Kiseleva, O., Zhmodik, S., PGE mineralization and melt composition of chromitites in Proterozoic ophiolite complexes of Eastern Sayan, Southern Siberia, Geoscience Frontiers (2016), http://dx.doi.org/10.1016/j.gsf.2016.04.003

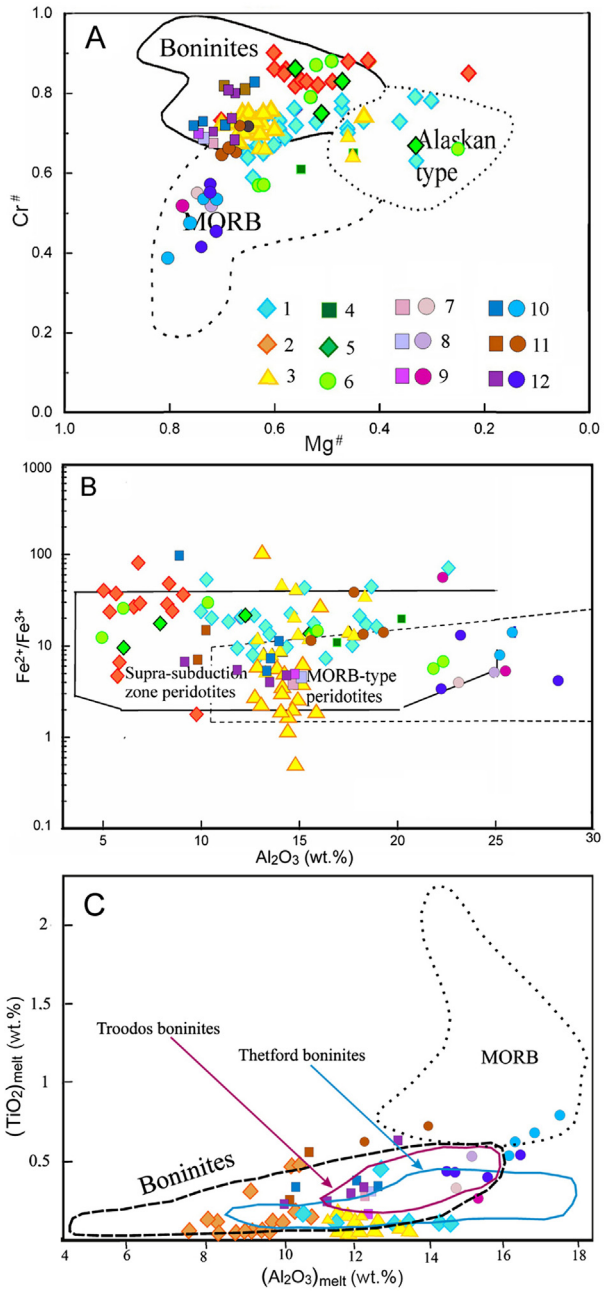

Figure 7. Compositional variation, showing chemical composition chromium spinels of chromite bodies from SEPES ophiolites, northern branch: 1–chromitite I, 2–chromitite II; southern branch: 3–chromitite I, 4–cpx harzburgite, 5–harzburgite, 6–dunite, 7–12 chromitites from world-wide ophiolite complexes (squares – high-Cr; circles – high-Al) are shown for comparison: 7–Troodos, 8–Oman, 9–New Caledonia, 10–Elekdag ophiolite, 11–Wadi Al Hwanet, north-western Saudi Arabia, 12–south-eastern Turkey; data sources from: Prichard and Lord., 1990; Proenza et al., 1999; Garutti, 2004 (database); Ahmed et al., 2012; Gonzales-Jiménez et al., 2012; Rollinson and Adetunji, 2013; Akmaz et al., 2014; (A) $Cr^{\#}$ versus $Mg^{\#}$, fields are from Barnes and Roeder (2001); (B) Fe^{2+}/Fe^{3+} versus Al_2O_3, fields are from Kamenetsky et al. (2001); (C) $(Al_2O_3)_{melt}$ vs. $(TiO_2)_{melt}$ of the melt calculated as in equilibrium with chromite from podiform chromitites of SEPES ophiolites. Fields for boninites (Jenner, 1981; Walker and Cameron, 1983; Kamenetsky et al., 2002), Troodos boninites (Cameron, 1985), Thetford boninites (Page and Barnes, 2009) and MORB (Shibata et al., 1979; Le Roex et al., 1987; Presnall and Hoover, 1987).

melts for the Cr-spinels with medium Al_2O_3 in northern and southern branches are: $(Al_2O_3)_{melt}$ = 10.5–14.5 and 11–13.5 wt.%; $(TiO_2)_{melt}$ = 0.01–0.44 and 0.01–0.15 wt.%; $(Fe/Mg)_{melt}$ = 0.45–1.81 and 0.34–1.09, respectively. For Cr-spinels with *low* Al_2O_3 in northern branch, the $(Al_2O_3)_{melt}$ = 8–10.5 wt.%, $(TiO_2)_{melt}$ = 0.01–0.25 wt.%, $(Fe/Mg)_{melt}$ = 0.47–2.39. For the accessory Cr-spinels, $(Al_2O_3)_{melt}$ = 7–14 wt.%, $(TiO_2)_{melt}$ = 0–0.35 wt.%, and these values overlap for different rocks (cpx-bearing harzburgites, harzburgites, dunites). These values correspond to boninite melts and only some of them have an affinity to MORB-like melts. On the $(Al_2O_3)_{melt} - (TiO_2)_{melt}$ discrimination diagram these chromitites fall in the boninite field near to Thetford and Troodos boninites.

Accordingly, we assume that high-Cr chromitites of northern branch could have crystallized from boninitic melts in a supra-subduction environment. Chromitites from the southern branch might have formed within a mid-ocean spreading zone with a subsequent change to a subduction environment forming low-Al Cr-spinels, as is typical of high-Al chromitites from other ophiolite complexes.

6.2. Different types of PGE distribution in chromitites

Different types of chromitites and PGE mineralization in single ophiolitic massifs have been investigated by many workers (Prichard and Lord, 1993; Rollinson, 2008; Uysal et al., 2009; Ahmed et al., 2012; Donmez et al., 2014). Several compositionally different types of chromitites and PGE mineralization have been recognized in the SEPES ophiolites.

Chromitites from the northern and southern branches of the SEPES ophiolites show differences in PGE distribution and mineralization. A fluid-saturated supra-subduction environment (Dick and Bullen, 1984) can explain the extreme fractionation of the PGE. Release of the PGE from their mantle source to the melt depends on the style of melting and the stage of dissociation of PGE in carrier phases (Mungall et al., 2006). The high concentration of PGE in high-Cr chromitites might be a result of a critical melting degree of 20–25% of the mantle (Prichard et al., 2008). Enrichment in PPGE, together with high IPGE contents in the same chromite deposits, may be attributed to a second stage of melting and formation of the enriched PGE-saturated melt (Hamlyn and Keays, 1986; Prichard et al., 1996), which is accompanied by the formation of Pt-Os-Ir-Ru solid solutions and other Pt-bearing phases (Kiseleva et al., 2014).

The PGE abundances and the Cr-spinel chemistry are useful indicators of the degree of partial melting and sulfur saturation in the primary melt (Nakagawa and Franco, 1997).

6.3. PGM formation in chromitites

Solid solutions of Os-Ir-Ru and laurite (RuS_2) form in the upper mantle together with Cr-spinel. Combined crystallization of the solid solutions Os-Ir-Ru and laurite occurs at $T \sim 1200–1250$ °C and log $fS_2 = -0.39$ to 0.07 (Andrews and Brenan, 2002). Primary laurite was more Os-rich than the observed values, as shown by the presence of an emulsion of micro-particles of native osmium in laurite, formed during desulfurization. In sites with high concentration of Os (up to 14 wt.%), sulfur content is decreased. Originally, there was a solid solution laurite-erlichmanite (RuS_2 - OsS_2). Osmium was released from solid solution during the desulfurization process whereas ruthenium, having a maximum affinity to sulfur, was retained.

Zonation is observed in the Os-Ir-Ru solid solutions. Near the center, they are replaced by irarsite, whereas in the outer rim zone they are replaced by laurite. This may be due to the enrichment of ruthenium towards rim of the grain. Besides iridium and ruthenium have various degrees of affinity with S and As, some of the laurite could be formed together with the irarsite. The (Os-Ir-Ru-Rh)AsS minerals formed in the post magmatic stage under the influence of S, As-bearing fluids.

Please cite this article in press as: Kiseleva, O., Zhmodik, S., PGE mineralization and melt composition of chromitites in Proterozoic ophiolite complexes of Eastern Sayan, Southern Siberia, Geoscience Frontiers (2016), http://dx.doi.org/10.1016/j.gsf.2016.04.003

Table 3
Calculated parental melt composition for chromian spinels from chromitite I and chromitite II types in northern and southern branches of SEPES ophiolites.

	1	2	3	4	5	6	7	8	9	10	11	12	13	14	15
	BC236/1	BC-159	OK-14/49	BC-237	BC-127	BC50-04	BC-63	BC-334	BC-52	K-61/5	OK-37	D10-2	BC-19	OK-38	BC-161
Al_2O_3	22.61	16.5	12.73	18.44	17.5	14.35	5.7	4.46	6.95	10.2	9.17	6.6	10.76	7.25	8.54
TiO_2	0.03	0.29	0.04	0.03	0.03	0.002	0.04	0	0	0.32	0.04	0	0.07	0	0.04
$Mg^{\#}$	0.64	0.63	0.43	0.62	0.6	0.46	0.42	0.5	0.46	0.48	0.55	0.23	0.38	0.38	0.58
$Al^{\#}$	0.41	0.31	0.25	0.34	0.32	0.28	0.11	0.09	0.14	0.2	0.18	0.14	0.21	0.14	0.17
$Cr^{\#}$	0.59	0.67	0.73	0.65	0.67	0.69	0.88	0.9	0.82	0.8	0.81	0.85	0.77	0.84	0.82
$Fe^{3+\#}$	0	0.02	0.03	0.01	0.01	0.03	0.01	0.01	0.04	0	0.01	0.01	0.02	0.01	0.02
$(Al_2O_3)_{melt}$	14.5	12.68	11.43	13.32	13.07	12.01	8.2	7.41	8.9	10.43	9.99	8.71	10.67	9.06	9.69
$(TiO_2)_{melt}$	0.07	0.44	0.08	0.07	0.07	0.01	0.08	0.01	0.01	0.48	0.09	0.01	0.13	<0.01	0.09
$(Fe/Mg)_{melt}$	0.55	0.5	1.08	0.56	0.57	0.97	0.95	0.67	0.83	0.84	0.61	2.39	1.23	1.18	0.54

	16	17	18	19	20	21	22	23	24	25	26	27	28	29	30
	BC-21/1	BC-349	BC-8	BC-17	K-34	K-35	K-40	K-43	K-96	BC-68	K-93	BC6526	BC6755	BC6756	BC6758
Al_2O_3	7.35	14.83	12.82	13.08	13.62	14.08	16.03	14.75	18.51	14.11	17.79	14.08	15.38	14.78	12.58
TiO_2	0.17	0.07	0.08	0.05	0.07	0.05	0.05	0.07	0.01	0.03	0.03				
$Mg^{\#}$	0.59	0.62	0.63	0.64	0.65	0.64	0.67	0.63	0.56	0.65	0.46	0.65	0.66	0.64	0.63
$Al^{\#}$	0.14	0.28	0.24	0.25	0.26	0.26	0.3	0.28	0.34	0.26	0.34	0.26	0.29	0.28	0.24
$Cr^{\#}$	0.85	0.72	0.74	0.73	0.72	0.71	0.68	0.71	0.64	0.73	0.64	0.72	0.7	0.72	0.75
$Fe^{3+\#}$	0	0	0.02	0.02	0.02	0.02	0.02	0.01	0.02	0.01	0.02	0.02	0.02	0.01	0.02
$(Al_2O_3)_{melt}$	9.11	12.18	11.47	11.32	11.76	11.92	12.58	12.15	13.35	11.93	13.13	11.92	12.36	12.16	11.38
$(TiO_2)_{melt}$	0.29	0.14	0.15	0.11	0.13	0.11	0.1	0.14	0.03	0.07	0.06	0.01	0.01	0.01	0.01
$(Fe/Mg)_{melt}$	0.5	0.52	0.47	0.45	0.43	0.46	0.42	0.48	0.72	0.45	1	0.44	0.44	0.46	0.47

	31	32	33	34	35	36	37	38	39	40	41	42	43	44	45
	BC1813	BC1816	OK1014	O10a1-1	O10an25	O10an63	OK-25/6	OK-8/2	OK-12/2	OK-21/3	OK-21/9	OK-44/1	OK-12/1	OK-13/2	OK-45/2
Al_2O_3	13.98	14.84	13.65	14.18	12.46	15.68	16.92	21.84	22.32	7.95	6.07	15.59	4.98	6.04	15.96
TiO_2							0.08	0.13	0.22	0.07	0.13	0.1	0.12	0.2	0.06
$Mg^{\#}$	0.64	0.6	0.64	0.7	0.66	0.63	0.45	0.62	0.63	0.47	0.56	0.33	0.49	0.52	0.25
$Al^{\#}$	0.26	0.28	0.26	0.26	0.23	0.29	0.32	0.4	0.41	0.16	0.12	0.31	0.1	0.12	0.31
$Cr^{\#}$	0.72	0.71	0.73	0.72	0.75	0.71	0.65	0.57	0.57	0.83	0.86	0.67	0.88	0.87	0.66
$Fe^{3+\#}$	0.02	0.01	0.01	0.02	0.01	0	0.02	0.03	0.03	0.02	0.02	0.02	0.02	0.01	0.03
$(Al_2O_3)_{melt}$	11.89	12.18	11.77	11.96	11.33	12.46	12.86	14.29	14.42	9.41	8.42	12.43	7.76	8.4	12.55
$(TiO_2)_{melt}$	0.01	0.01	0.01	0.01	0.01	0.01	0.15	0.23	0.35	0.14	0.23	0.18	0.21	0.32	0.12
$(Fe/Mg)_{melt}$	0.47	0.56	0.46	0.35	0.41	0.51	1.07	0.57	0.56	0.83	0.55	1.74	0.7	0.65	2.56

	46	47	48	49	50	51	52	53	54	55	56	57	58	59
			Tr-1	Tr-2	Om-1	Om-2	N Cal-1	N Cal-2	El-I	El-II	Wadi-I	Wadi-II	S T-I	S T-II
Al_2O_3			14.87	23.55	15.33	25.11	25.80	15.20	9–14.3	25.3–34.8	9.9–10.8	15.7–19.4	9.4–14.9	22.3–31.7
TiO_2			0.15	0.19	0.17	0.35	0.14	0.07	0.2–0.3	0.2–0.3	0.01–0.05	0.13–0.4	0.09–0.2	0.07–0.3
$Mg^{\#}$			0.66	0.69	0.67	0.65	0.73	0.69	0.4–0.7	0.6–0.8	0.6–0.7	0.6–0.7	0.4–0.7	0.6–0.7
$Al^{\#}$			0.28	0.42	0.29	0.45	0.45	0.28	0.2–0.3	0.5–0.6	0.19–0.2	0.3–0.4	0.2–0.3	0.3–0.6
$Cr^{\#}$		0.1–0.5	0.68	0.53	0.68	0.51	0.52	0.68	0.7–0.8	0.4–0.5	0.79–0.8	0.6–0.7	0.7–0.8	0.4–0.6
$Fe^{3+\#}$			0.04	0.05	0.04	0.04	0.03	0.03	0–0.03	0.02–0.03	0.01–0.03	0.01	0.02–0.08	0.01–0.07
$(Al_2O_3)_{melt}$	10.6–14.4	~15	12.19	14.74	12.35	15.14	15.31	12.30	10.4–12.7	15.6–16.9	10.2–10.7	12.2–13.9	10–12.2	14.5–16.5
$(TiO_2)_{melt}$	0.1–0.5	0.3–2.2	0.26	0.31	0.28	0.51	0.24	0.14	0.24–0.37	0.52–0.79	0.23–0.55	0.25–0.55	0.18–0.3	0.06–0.48
$(Fe/Mg)_{melt}$	0.7–1.4	1.2–1.6	0.42	0.43	0.41	0.53	0.38	0.38	0.61–1.81	0.43–0.81	0.76–1.17	0.72–1.12	0.42–0.55	0.4–0.62

Comments: (authors data) from northern branch: 1–6 ore chromian spinels medium-$Al^{\#}$, 7–16 low-$Al^{\#}$; from southern branch: 17–36 ore chromian spinels medium-$Al^{\#}$; (data from Antsiferova, 2006): 37–45 accessory chromian spinels in: 37 Cpx-bearing harzburgites, 38–42 harzburgites, 43–45 dunites; 46 boninite (SSZ) (Wilson, 1989); 47 MORB (Wilson, 1989; Kamenetsky et al., 2001); SSZ – supra-subduction zone, MORB – mid-ocean ridge basalt; 48–59 chromitites from world-wide ophiolitic complex (data source Garutti, 2004. database; Prichard and Lord, 1990; Proenza et al., 1999; Gonzales-Jiménez et al., 2012; Rollinson and Adetunji, 2013): 48, 49 chromitites Troodos high-Cr, high-Al; 50, 51 chromitites Oman high-Cr, high-Al; 52, 53 chromitites New Caledonia high Cr, high Al; 54, 55 chromitites Elekdag ophiolite; 56, 57 chromitite Wadi Al Hwanet, northwestern Saudi Arabia (Ahmed et al., 2012); 58, 59 chromitites from the southeastern Turkey (Akmaz et al., 2014).
$Mg^{\#} = Mg/(Mg + Fe^{2+})$; $(Al_2O_3)sp$ (wt.%) = 0.035 $(Al_2O_3)^{2.42}_{melt}$; $(TiO_2)melt$ (wt.%) = $(TiO_2)^{0.82524}sp * e^{0.20203}$; $\ln (FeO/MgO)_{sp} = 0.47-1.07*Al^{\#}_{sp}+0.64*Fe^{3+\#} + \ln (FeO/MgO)_{melt}$ (Maurel and Maurel, 1982); F (degree of partial melt) = 10 $\ln(Cr^{\#})$ + 24 (Hellebrand et al., 2001).

Mantle peridotites have been exposed with mantle-derived reduced fluids, as indicated by the widespread occurrences of highly carbonaceous graphitized ultrabasic rocks and serpentinites. Fluid inclusions in the carbonaceous graphitized ultrabasic rocks contain CO, CO_2, CH_4, N_2. The $\delta^{13}C$ isotopic composition is −7.4 to −14.5‰, broadly corresponding to mantle carbon (Savelyeva et al., 1998; Zhmodik et al., 2004).

The microstructure features of PGM reflect processes of remobilization. Remobilization of the PGE with the participation of reduced mantle fluids takes place during desulfurization and dearsenization followed by formation of "primary" IPGE. In turn the influence of metasomatic asthenospheric fluids leads to dissolution of mantle sulfides and sulfoarsenides (Os-Ir-Ru) and formation of the "secondary" minerals of native osmium, ruthenium, RhNiAs, (Ir, Ni, Fe) (Kiseleva et al., 2014). Based on the chemical compositions and microstructures of the Os-Ir-Ru solid solutions and sulfoarsenides of Os-Ir-Ru, it was observed that Os had the lowest chemical affinity with S and As, thus Os releases initially from S, As and finally forms dispersed aggregates of native osmium (Os > 80 wt.%).

Changes of the redox state from reducing to oxidizing conditions were followed by formation of the PGE together with the As, Sb, Sn and Ni arsenides, ferrichromite, Cr-magnetite. The latter association indicates the redistribution of chromite and PGM along with the formation of new minerals within the ultramafic substrate under crustal conditions.

Please cite this article in press as: Kiseleva, O., Zhmodik, S., PGE mineralization and melt composition of chromitites in Proterozoic ophiolite complexes of Eastern Sayan, Southern Siberia, Geoscience Frontiers (2016), http://dx.doi.org/10.1016/j.gsf.2016.04.003

7. Conclusions

(1) Chemical compositions of the Cr-spinels, the mineralogical and geochemical features of the PGE, and published geochronological and petrochemical data of the intrusive and extrusive rocks indicate the differences in the environments of formation of the Proterozoic SEPES ophiolites in northern and southern ophiolite branches.
(2) Peridotites of these ophiolite complexes experienced a long process of evolution in the lithospheric mantle, which includes repeated partial melting processes. This was followed by the formation of high $Cr^{\#}$ chromite in podiform chromitites.
(3) High-Cr chromitites, with high-PGE (IPGE + PPGE) concentrations, formed due to high degrees of partial melting (20% or more) from boninite melt in fluid-rich supra-subduction environments. The chromitites with the mean-Al content of chromite might have formed with the interaction of MORB-type melts followed by subsequent modifications and repeated stages of melting in subduction environments.
(4) Enrichment in PPGE, together with high content of IPGE in the same chromite deposits, may be attributed to a second stage of melting and formation of PGE-enriched and saturated melts. Enrichment in PPGE leads to the formation of Pt-Os-Ir-Ru solid solutions and other Pt-bearing phases.
(5) Different stages of the PGE mineralization include (i) the magmatic stage, where the chromite formed together with the alloys Os-Ir-Ru, laurite; (ii) the post-magmatic stage, where the PGE sulfoarsenides formed. Under the influence of reduced mantle fluids, desulfurization and dearsenization, the primary PGMs were replaced by the secondary PGMs.

Acknowledgments

This study was supported by RFBR grant Nos. 16-05-00737 A, 16-05-00860 A, and 15-05-06950 A, scientific school – 7201.2012.5, project SB RAS No. 89. We are also grateful to Prof. H. Downes for the language correction.

References

Agafonov, L.V., Kuzhuget, K.S., Oydup, Ch.K., Stupakov, S.I., 1993. Native Metals in Ultramafic Massifs of Tuva. UIIM SB RAN, Novosibirsk, 86 p (in Russian).
Ahmed, A.H., Arai, S., 2002. Platinum-group Element Geochemistry in Podiform Chromitites and Associated Peridotites of the Precambrian Ophiolite, Eastern Desert, Egypt. Proceedings, 9th International Platinum Symposium, Billings, Montana, pp. 1–4.
Ahmed, H.A., 2007. Diversity of platinum-group minerals in podiform chromitites of the late Proterozoic ophiolite, Eastern Desert, Egypt: Genetic implication. Ore Geology Reviews 32, 1–19.
Ahmed, A.H., Arai, S., 2003. Platinum-group minerals in podiform chromitites of the Oman ophiolite. Canadian Mineralogist 41, 597–616.
Ahmed, A.H., Harbi, H.M., Habtoor, A.H., 2012. Compositional variations and tectonic settings of podiform chromitites and associated ultramafic rocks of the neoproterozoic ophiolites at Wadi Al Hwanet, northwestern Saudi Arabia. Journal of Asian Earth Sciences 5, 118–134.
Ahmed, H.A., 2013. Highly depleted harzburgite-dunite-chromitite complexes from the Neoproterozoic ophiolite, south Eastern Desert, Egypt: A possible recycled upper mantle lithosphere. Precambrian Research 233, 173–192.
Akmaz, R.M., Uysal, I., Saka, S., 2014. Compositional variations of chromite and solid inclusions in ophiolitic chromitites from the southeastern Turkey: implications for chromitite genesis. Ore Geology Reviews 58, 208–224.
Andrews, D.R.A., Brenan, J.M., 2002. Phase-equilibrium constraints of the magmatic origin of laurite and Os-Ir alloy. Canadian Mineralogist 40, 1705–1716.
Antsiferova, T.N., 2006. Petrology and Mineralogy of Ultramafic Rocks from the Ospa Massif. PHD dissertation (Geol.-Mineral.), extended abstract, Ulan-Ude, 24 p (in Russian).
Ballhaus, C., 1998. Origin of podiform chromite deposits by magma mingling. Earth and Planetary Science Letters 156, 185–193.
Barnes, S.J., Roeder, P.L., 2001. The range of spinel composition in terrestrial mafic and ultramafic rocks. Journal of Petrology 42, 2279–2302.
Barnes, S.J., Naldrett, A.J., Gorton, M.P., 1985. The origin of the fractionation of platinum-group elements in terrestrial magmas. Chemical Geology 53, 303–323.
Cameron, W.E., 1985. Petrology and origin of primitive lavas from the Troodos ophiolite Cyprus. Contributions to Mineralogy and Petrology 89, 239–255.
Derbyshire, E.J., O'Driscoll, B., Lenaz, D., Gertisser, R., 2013. Compositionally heterogeneous podiform chromitite in the Shetland Ophiolite Complex (Scotland): implications for chromitite petrogenesis and late-stage alteration in the upper mantle portion of a supra-subduction zone ophiolite. Lithos 162–163, 279–300.
Dick, H.J.B., Bullen, T., 1984. Chromium-spinel as a petrogenetic indicator in abyssal and alpine-type peridotites and spatially associated lavas. Contributions to Mineralogy and Petrology 86, 54–76.
Dilek, Y., 2003. Ophiolite pulses, mantle plumes, and orogeny. In: Dilek, Y., Robinson, P.T. (Eds.), Ophiolites in Earth History, Geological Society of London, Special Publication, 218, pp. 9–19.
Dobretsov, N.L., Ignatovich, V.I., 1989. Geology and Ore-bearing Zones of Eastern Sayan. Nauka, Novosibirsk, 126 p (in Russian).
Dobretsov, N.L., Konnikov, E.G., Medvedev, V.N., Sklyarov, E.V., 1985. Ophiolites and olistostromes of East Sayan. In: Dobretsov, N.L. (Ed.), Riphean-Lower Paleozoic Ophiolites of North Eurasia. Nauka, Novosibirsk, pp. 34–57 (in Russian).
Donmez, C., Keskin, S., Gunay, K., Colakoglu, A.O., Ciftci, Y., Uysal, I., Turkel, A., Yildirim, N., 2014. Chromite and PGE geochemistry of the Elekdag Ophiolite (Kastamonu, Northern Turkey): Implication for deep magmatic processes in a supra-subduction zone setting. Ore Geology Reviews 57, 216–228.
Fedotova, A.A., Khain, E.V., 2002. Tectonics of south Eastern Sayan and its position in Ural-Mongol belt. Science World, Works of GIN RAS 537, 176 (in Russian).
Garuti, G., Zaccarini, F., 1997. In situ alteration of platinum-group minerals at low temperature: evidence from serpentinized and weathered chromitite of the Vourinos complex, Greece. Canadian Mineralogist 35, 611–626.
Garutti, G., 2004. Chromite-platinum-group element magmatic deposits. In: Vivo, De B., et al. (Eds.), Geology, Encyclopedia of Life Support Systems (EOLSS). UNESCO, Eolss Publisher, Oxford, UK. http://www.eolss.net.
Gonzales-Jimenez, J., Auge, T., Gervilla, F., Baily, L., Proenza, J.A., Griffin, W.L., 2012. Mineralogy and geochemistry of platinum-rich chromitites from the mantle-crust transition zone at Ouen Island, New Caledonia Ophiolite. The Canadian Mineralogist 49 (6), 1549–1569.
González-Jiménez, J.M., Proenza, J.A., Gervilla, F., Melgarejo, J.C., Blanco-Moreno, J.A., Ruiz-Sánchez, R., Griffin, W.L., 2011. High-Cr and high-Al chromitites from the Sagua de Tánamo district, Mayarí-Cristal ophiolitic massif (eastern Cuba): constraints on their origin from mineralogy and geochemistry of chromian spinel and platinum-group elements. Lithos 125, 101–121.
Grieco, G., Merlini, A., Cazzaniga, A., 2012. The tectonic significance of PGM-bearing chromitites at the Ranomena mine, Toamasina chromite district, Madagascar. Ore geology Reviews 44, 70–81.
Hamlyn, P.R., Keays, R.R., 1986. Sulfur saturation and second stage melts; application to the Bushveld Pt metal deposits. Economic Geology 81, 1431–1445.
Harris, D.C., Cabri, L.J., 1991. Nomenclature of platinum-group-element alloys: review and revision. Canadian Mineralogist 29, 231–237.
Hellebrand, E., Snow, J.E., Dick, H.J.B., Hofmann, A.W., 2001. Coupled major and trace elements as indicators of the extent of melting in mid-ocean-ridge peridotites. Nature 410, 677–681.
Jenner, G.A., 1981. Geochemistry of high-Mg andesites from Cape Vogel, Papua New Guinea. Chemical Geology 33, 307–332.
Kamenetsky, V., Crawford, A.J., Meffre, S., 2001. Factors controlling chemistry of magmatic spinel: an empirical study of associated olivine, Cr-spinel and melt inclusions from primitive rocks. Journal of Petrology 42, 655–671.
Kamenetsky, V.S., Sobolev, A.V., Eggins, S.M., Crawford, A.J., Arculus, R.J., 2002. Olivine- enriched melt inclusions in chromites from low-Ca boninites, Cape Vogel, Papua New Guinea: evidence for ultramafic primary magma, refractory mantle source and enriched components. Chemical Geology 183, 287–303.
Kiseleva, O.N., Zhmodik, S.M., Damdinov, B.B., Agafonov, L.V., Belyanin, D.K., 2014. Composition and evolution of PGE mineralization in chromite ores from the Il'chir ophiolite complex (Ospa-Kitoi and Khara-Nur areas, East Sayan). Russian Geology and Geophysics 55, 259–272.
Kuźmichev, A.B., Larionov, A.N., 2013. Neoproterozoic island arcs in East Sayan: duration of magmatism (from U–Pb zircon dating of volcanic clastics). Russian Geology and Geophysics 54 (1), 34–43.
Le Roex, A.P., Dick, H.J.B., Gulen, L., Reid, A.M., Erlank, A.J., 1987. Local and regional heterogeneity in MORB from the mid-Atlantic ridge between 54.5°S and 51°S: evidence for geochemical enrichment. Geochimica et Cosmochimica Acta 51, 541–555.
Liipo, J., Vuollo, J., Nykanen, V., Piirainen, T., Pekaarinen, L., Tuokko, J., 1995. Chromites from the early Proterozoic Outkumpu-Jormua ophiolite belt: a comparison with chromites from Mezozoic ophiolites. Lithos 36, 15–27.
Maurel, C., Maurel, P., 1982. Étude expérimentale de la distribution de l'aluminium entre bain silicaté basique et spinelle chromifère. Implications pétrogénétiques: teneur en chrome des spinelles. Bulletin de Minéralogie 105, 197–202.
Melcher, F., Grum, W., Simon, G., Thalhammer, T.V., Stumpfl, E.F., 1997. Petrogenesis of the Ophiolitic Giant Chromite Deposits of Kempirsai, Kazakhstan: a study of solid and fluid inclusions in chromite. Journal of Petrology 38, 1419–1458.
Mungall, J.E., Hanley, J.J., Arndt, N.T., Debecdelievre, A., 2006. Evidence from meimechites and other low-degree mantle melts for redox controls on mantle – crust fractionation of platinum-group elements. Proceedings of the National Academy of Sciences 103, 12695–12700.
Nakagawa, M., Franco, H.E.A., 1997. Placer Ru-Os-Ir alloys and sulfides: indicators of sulfar fugacity in an ophiolite? Canadian Mineralogist 38, 1419–1458.

Naldrett, A.J., 2010. Secular variation of magmatic sulfide deposits and their source magmas. Economic Geology 105, 669–688.
Orsoev, D.A., Tolstykh, N.D., Kislov, E.V., 2001. $PtCu_3$ composition mineral from chromitites of Ospinsko-Kitoisky ultramafic massif (Eastern Sayans). Zapiski VMO 130 (4), 61–70 (in Russian).
O'Driscoll, B., Day, J.M.D., Walker, R.J., Daly, J.S., McDonough, W.F., Piccoli, P.M., 2012. Chemical heterogeneity in the upper mantle recorded by peridotites and chromitites from the Shetland Ophiolite Complex, Scotland. Earth and Planetary Science Letters 333–334, 226–237.
Page, P., Barnes, S.J., 2009. Using trace elements in chromites to constrain the origin of podiform chromitites in the Thetford Mines Ophiolite, Québec, Canada. Economic Geology 104, 997–1018.
Pavlov, N.V., Kravchenko, G.G., Chuprynina, I.I., 1968. Chromites from the Kempirsai Pluton. Nauka, Moscow (in Russian).
Podlipsky, M.Yu., Krivenko, A.P., Polyakov, G.V., 2004. Platinum-palladium mineralization in chromite ores from ultrabasic rocks of the western Sayan region. Doklady Earth Sciences 396 (4), 508–511.
Presnall, D.C., Hoover, J.D., 1987. High pressure phase equilibrium constraints on the origin of mid-ocean ridge basalts. Geochemical Society Special Paper 1, 75–89.
Prichard, H.M., Fisher, P.C., Nearly, C.R., Ohara, M.J., 2008. PGE-rich podiform chromitites in the Al Ays ophiolite complex, Saudi Arabia: an example of critical mantle melting to extract and concentrate PGE. Economic Geology 103, 1507–1529.
Prichard, H.M., Lord, R.A., 1990. Platinum and palladium in the Troodos ophiolite complex, Cyprus. Canadian Mineralogist 28 (3), 607–617.
Prichard, H.M., Lord, R.A., 1993. An overview of the PGE concentrations in the Shetland ophiolite complex. In: Prichard, H.M., Alabaster, T., Harris, N.B.W., Neary, C.R. (Eds.), Magmatic Processes and Plate Tectonics, Geological Society of London, Special Publication, 76, pp. 273–294.
Prichard, H.M., Lord, R.A., Neary, C.R., 1996. A model to explain the occurrence of Pt and Pd-rich ophiolite complexes. Journal of Geological Society of London 153, 323–328.
Proenza, J., Gervilla, F., Melgarejo, J.C., Bodinier, J.L., 1999. Al- and Cr-rich chromitites from the Mayari–Baracoa Ophiolitic Belt (eastern Cuba):consequence of interaction between volatile-rich melts and peridotite in suprasubduction mantle. Economic Geology 94, 547–566.
Rehkämper, M., Halliday, A.N., Barford, D., Godfrey, J.F., Dawson, J.B., 1997. Platinum-group element abundance patterns in different mantle environments. Science 278, 1595–1598.
Rollinson, H., 2008. The geochemistry of mantle chromitites from the northern part of the Oman ophiolite: inferred parental melt composition. Contributions to Mineralogy and Petrology 156, 273–288.
Rollinson, H., Adetunji, J., 2013. Mantle podiform chromitites do not form beneath mid-ocean ridges: a case study from the Moho transition zone of the Oman ophiolite. Lithos 177, 314–327.
Savelyeva, V.B., Zvonkova, N.G., Yu.V, Anikina, 1998. Carbonaceous tectonites of the Ospa-Kitoi ultrabasic-rock massif (East Sayan). Russian Geology and Geophysics 39 (5), 598–611 (in Russian).
Shibata, T., Thompson, G., Frey, F.A., 1979. Tholeiitic and alkali basalts from the mid Atlantic ridge at 43°N. Contributions to Mineralogy and Petrology 70, 127–141.
Tsoupas, G., Economou-Eliopoulos, M., 2008. High PGE contents and extremely abundant PGE minerals hosted in chromitites from Veria ophiolite complex, northern Greece. Ore Geology Reviews 33, 3–19.
Uysal, I., Tarkian, M., Sadiklar, M.B., Zaccarini, F., Meisel, T., Garuti, G., Heidrich, S., 2009. Petrology of Al- and Cr-rich ophiolitic chromitites from the Muğla, SW Turkey: implications from composition of chromite, solid inclusions of platinum-group mineral, silicate, and base-metal mineral, and Os-isotope geochemistry. Contributions to Mineralogy and Petrology 158 (5), 659–674.
Walker, D.A., Cameron, W.E., 1983. Boninite primary magmas: evidence from the Cape Vogel Peninsula, PNG. Contributions to Mineralogy and Petrology 83, 150–158.
Wilson, M., 1989. Igneous Petrogenesis. Unwin Hyman, London, 446 p.
Zhmodik, S.M., Mironov, A.G., Agafonov, L.V., Zhmodik, A.S., Pavlov, A.L., Moroz, T.N., Airiyants, E.V., Kulikov, Yu.L., Borovikov, A.A., Ponomarchuk, V.A., Damdinov, B.B., 2004. Carbonization of east Sayan ultrabasic rocks and Au-Pd-Pt mineralization. Russian Geology and Geophysics 45 (2), 210–225.
Zhmodik, S.M., Postnikov, A.A., Buslov, M.M., Mironov, A.G., 2006. Geodynamics of the Sayan-Baikal-Muya accretion-collision belt in the neoproterozoic-early paleozoic and regularities of the formation and localization of precious-metal mineralization. Russian Geology and Geophysics 47 (1), 187–201.
Zhmodik, S., Kiseleva, O., Belyanin, D., Damdinov, B., Airiyants, E., Zhmodik, A., 2014. PGE Mineralization in Ophiolites of the Eastern Sayan (Russia), 12th International Platinum Symposium, 11–14 August 2014, Yekaterinburg, Russia. IGGU-BRAS, Yekaterinburg, pp. 221–222.
Zhou, M.-F., Sun, M., Keays, R.R., Kerrich, R.W., 1998. Controls of platinum-group elemental distributions of podiform chromitites: a case study of high-Cr and high-Al chromitites from Chinese orogenic belts. Geochimica et Cosmochimica Acta 62, 677–688.

Please cite this article in press as: Kiseleva, O., Zhmodik, S., PGE mineralization and melt composition of chromitites in Proterozoic ophiolite complexes of Eastern Sayan, Southern Siberia, Geoscience Frontiers (2016), http://dx.doi.org/10.1016/j.gsf.2016.04.003